

## ORIGINAL ARTICLE

# Material Properties Analysis with Addition of Nanofibres for Air Intake Filtration in Internal Combustion Engines

T. Dziubak

Faculty of Mechanical Engineering, Military University of Technology, 00-908 Warsaw, Poland  
Phone: +504574057; Fax: 48 261837121

**ABSTRACT** – The aim of this study is to provide an experimental properties evaluation of a standard filter material (cellulose) and materials with fiber layer addition with small diameters (nanofibers). Filter media, including cellulose, used in the internal combustion engine inlet air filtration are made of high diameter fibres, approx. 15  $\mu\text{m}$ . Significantly higher separation and filtration efficiency performance are obtained for materials with lower fibre diameters (nanofibres), however, at the expense of a significantly higher pressure drop, affecting the engine performance. Filter media manufacturers mainly specify the structure parameters (pore size, air permeability and thickness), without giving any information on the dust filtration performance and rate. The literature includes test results for models of different filter media structures. Filtration process modelling using polydisperse dust with particles of different shape and density and irregular filter media structure is possible using advanced computer techniques, however, the process is complex and requires many simplifications. Test results can be applied directly in the automotive industry. The data can be obtained by experimental tests on filter medium specimens, complete filter elements or air filters which are costly and time-consuming tests, however, those test methods are the most reliable. Conditions and testing methodology for intake air filter materials used in internal combustion engines were developed. Filtration and flow resistance efficiency and accuracy were done depending on test dust mass stopped per unit area. Tested materials filtration efficiency was assessed by a filtration quality factor, which includes experimentally determined efficiency and accuracy as well as flow resistance values. Much higher efficiency and filtration accuracy of dust grains below 5  $\mu\text{m}$  in filtration materials with nanofibers addition compared to standard filtration material (filter paper) were demonstrated. For the same flow resistance values, filter materials with nanofibers addition accumulate smaller dust mass than standard filter paper. Usage of materials with nanofibers addition used in motor vehicles intake air filtration ensures their high efficiency and accuracy. It minimises its components wear, but at the expense of faster flow resistance increase, which shortens filter life and increases filter replacement frequency. Results obtained during the experimental research partly fill the gap when it comes to the basic material properties used in internal combustion engines intake air filter partitions production.

**ARTICLE HISTORY**Received: 13<sup>th</sup> Dec 2019Revised: 8<sup>th</sup> July 2020Accepted: 5<sup>th</sup> April 2021**KEYWORDS***Nanofibres;  
Separation efficiency;  
Filtration performance;  
Dust mass loading;  
Pressure drop*

## INTRODUCTION

Air taken from the atmosphere is the basic working factor of every internal combustion engine, which is a driving unit in motor vehicles, working machines, aeroplanes and helicopters. The engine needs a minimum of 14.5 kg of air to burn 1 kg of fuel. During operation in rated conditions, passenger car engines suck in 150-400  $\text{m}^3$  of air per hour. For truck engines, the value is 900-1400  $\text{m}^3/\text{h}$ , and for the engine of Leopard 2 tank, it is over 6,000  $\text{m}^3/\text{h}$ . Combustion engines suck in various pollutants with air. Mineral dust, which is lifted from the ground to a height of several meters by the movement of vehicles or by wind, is a commonly harmful air pollutant for operated technical devices.

Air dust concentration is a characteristic feature of polluted air, and its measure is the dust mass (in gram or mg) contained in 1  $\text{m}^3$  of atmospheric air. Typical concentrations can range from 0.01  $\text{mg}/\text{m}^3$  in clean rural environments and up to about 20  $\text{g}/\text{m}^3$  in desert heavy vehicle convoys [1]. The authors of the work [2] state that the dust concentration on highways ranges from 0.0004-0.1  $\text{g}/\text{m}^3$  to 0.03-8  $\text{g}/\text{m}^3$  when driving a column of vehicles on sandy terrain. Similar values of dust concentration in the air occur during the helicopter's take-off or landing at an accidental landing site. The rotating propeller lifts large amounts of mineral dust from the ground, which the engine then absorbs with the air. The highest dust concentration values are found low (0.5 m) above the ground. At the height of the propeller end of the CH-53 helicopter taking off, the dust concentration may have the value  $s = 3.33 \text{ g}/\text{m}^3$ , and at a distance of 30 m,  $s = 2.11 \text{ g}/\text{m}^3$  [3]. However, the actual dust concentration at the inlet to the engine intake system does not often exceed the value of 2.5  $\text{g}/\text{m}^3$  [1]. The concentration of dust in the air within the limits of 0.6-0.7  $\text{g}/\text{m}^3$  significantly reduces visibility, and at a

concentration of about  $1.5 \text{ g/m}^3$ , it is practically zero [4]. The following table (Table 1) provides typical dust concentrations for a variety of engine operating sites [1].

**Table 1.** Range of dust concentrations [1].

	Condition	Dust concentration ( $\text{mg/m}^3$ )
1	Average ambient	0.010-0.139
2	95 <sup>th</sup> percentile ambient	0.089
3	99 <sup>th</sup> percentile ambient	0.112
4	Paved roads	0.139-57
5	Dirt roads	0.139-6113
6	Dust storms	0.1-176
7	Worst dust storm	3000
8	0 visibility	883
9	20×0 visibility	17.657

The task of the inlet system in a motor vehicle's internal combustion engine is to deliver air to the engine cylinders in appropriate amounts and with appropriate parameters, in such a way as to ensure the correct course of the fuel combustion process in the engine cylinders [4-7]. An important task is to supply air with appropriate quality (cleanliness) to engine cylinders to minimise engine components wear. Engine wear is caused by dust particles of 1-40  $\mu\text{m}$ , and the most harmful particles occur in the range of 1-20  $\mu\text{m}$  [1, 8]. Dust suspended in the air, whose basic component is silica ( $\text{SiO}_2$ ), and which amount in the dust is in the range of 60-90%, at the same time has high hardness (7 on the Mohs scale) and is the most common cause of accelerated wear of such engine components as; piston rings, cylinder walls and piston [9]. As a result, there is a decrease in engine fill and power and an increase in exhaust gas blow-by into the crankcase. Authors [8] report that about 30% of pollutants getting into the engine may come out of the exhaust system along with exhaust gases, thus increasing the PM emission from the engine. Only 10-20% of the dust that enters the engine with the air through the intake system settles on the walls of the cylinder liner. Together with oil, this dust forms a kind of abrasive paste, which in contact with the engine connection surfaces; for example, piston-piston rings-cylinder (P-PR-C) causes abrasive wear. The most dangerous are dust particles whose diameter  $d_z$  is equal to the oil film thickness  $h_{min}$  between the two surfaces at a given moment. In typical combinations in the combustion engine, the oil film thicknesses vary in the range of  $h_{min}=0-50 \mu\text{m}$  [10]. Thus, all dust particles sucked in with the air cause accelerated wear.

Another task of the intake system is to damp the noise of the combustion process in the [11] engine and forcing the wave phenomena causing the so-called dynamic (resonant) supercharging in the desired engine operating ranges, thus increasing cylinder filling and engine power [12]. For this reason, work is constantly being carried out to (a) improve the engine filling process with fresh load by improving the design of the intake system and (b) improve the air intake filtration process by using more and more effective and precise filtration materials.

Authors of [5] believe that the airflow inside the intake system is disturbed by converging and diverging system components, leading to sudden acceleration and slowdown of the flow and cause excessive turbulence. Excessive flow resistance in the intake system affects the pressure drop effect and thus lower engine performance. The work investigates the aerodynamics of motorcycle intake systems depending on the airflow in the range of 50-130 CFM. A three-dimensional simulation of the flow in the motorcycle intake system was performed using computational fluid dynamics (CFD).

In [11], a simulation was carried out to improve the existing design of the air intake system for acoustic testing; to achieve better sound quality by modifying the resonators, air duct and air chamber volume of the air intake module. This study used a 1-dimensional simulation using commercial software correlated with a 1.6 litre naturally aspirated engine. The purpose of this test is to reduce engine noise at the air intake module tube without losing too much pressure drop. At the end of this study, the analysis identified the geometry of the air intake module with the resonator recommended for production and physical tests. The simulation result shows that the modified air intake module meets the purpose and meets the assumed parameters.

The authors of [6] believe that an increase in engine performance and a reduction in fuel consumption of a naturally aspirated engine can be achieved by optimising the geometry of intake system components - airbox. Important parameters in the design of the airbox geometry are the intake diameter, airbox volume, throttle body diameter and the length of the intake manifold. The optimisation process was carried out using the Box-Behnken method. Following optimal dimensions of intake system components have been determined: intake diameter 81.07 mm, airbox volume  $\text{dm}^3$ , throttle body diameter 44.63 mm and intake manifold length 425 mm. This allowed obtaining maximum engine performance (torque and power) and minimum fuel consumption.

The authors of [12] presented the influence of variable valve timing and valve lift on the performance in the internal combustion engine and fuel consumption. The lift and profile of the valves, which are the main factors affecting the dynamics of the waves and gases in the combustion chamber, were varied at all engine speeds to obtain an enhanced pressure wave to increase engine cylinders filling. As a result of changing the above parameters, the engine torque and power increased by an average of 6.02% over the entire range of engine operating speeds. The improvement in the lower speed range of 3000-4000 rpm is approximately 18.72%. Connection of variable valve lift (VVL) and variable valve timing (VVT) further reduces specific fuel consumption at all engine speeds, achieving an average reduction of 0.35%.

In [13], an effective method of improving diesel engine performance at low revolutions is by isolating the intake system components from hot engine components. The inlet air temperature was lowered. Results of experimental studies suggest that engine performance has increased significantly because of this. An insulated air intake system effectively reduces heat loss in the combustion engine by keeping the intake air temperature low. The degree of filling in the internal combustion engine increases with a decrease in the intake air temperature, mainly due to an increase in intake air density.

In [14], the individual and combined influence of the variable length of the inlet channel and inlet valves timing on the parameters of internal combustion engine at rotational speeds from 3000 rpm to 9000 rpm was examined. The combined effect obtained in this way shows an average power improvement of 7.02% over the entire engine speed range. Due to the coexistence of variable length intake channels and variable intake valve opening time, the number of changes required to increase engine performance is reduced, making the variable intake length assembly more workable.

In order to improve engine filling, the authors of [15] used the Helmholtz resonator (HR), which is one of the basic acoustic models and widely used in engineering works. In this study, the characteristics of the pulsating flow in the engine intake manifold with the participation of a Helmholtz resonator with a variable internal volume were investigated experimentally. Experiments were carried out on a straight intake pipe connected to the engine cylinder head. Using electronic control, the internal volume of the resonator was changed and adjusted to the frequency of the valves and to the natural frequency of the intake manifold. Results showed that the internal resonator volume and frequency tuning affect mass airflow in the intake system. For a constant volume, the average increase in mass flow rate was 17.8%, and when the volume was adjusted to valve frequency, the average increase was 24.7%.

The effect of tuning a pulsating sound wave produced over a wide speed range in the exhaust manifold on the power and torque of a single-cylinder GI engine was analysed in [16]. The simulation results are compared with standard data obtained during engine tests. There was an average 7% increase in torque and 6% increase in power with the continuous change in exhaust pipe length. With a constant change in exhaust pipe diameter, a 6% increase in torque and power is observed. Combining the changes in the length and exhaust pipe diameter resulted in an 8.5% increase in torque and a 9% increase in power, respectively.

The air filter with the intake is responsible for providing engine cylinders air with appropriate cleanliness. Passenger car engines are equipped with air filters, where the filter element is a cartridge made of pleated filter paper, which is the dominant filter material for intake air in modern combustion engines. During cars exploitation, impurities are retained on filter paper, which ensures air cleanliness supplied to the engine, and thus its durability. However, this causes a continuous pressure drop on the filter and in the intake system, which has a negative impact on the engine work in the form of filling and engine power drop. Criteria of air filter ending service life is reaching the value of the permissible filter resistance  $\Delta p_{fdop}$ . The filter cartridge should then be replaced with a new one, even though it still provides high efficiency and filtration accuracy. Such activity is most often performed after a certain mileage of the car or a specific time of engine work. Air filter durability is a technical compromise between pressure drop (car mileage), separation efficiency and filtration performance.

For this reason, experimental and numerical studies of pleated paper filter cartridges are constantly conducted in order to improve the filtering process of engine intake air [17-24]. Conducted research includes many parameters impact of the paper element, including pleat height and width, spaces between pleats, pleats shape, angle between pleats, filter medium thickness, airflow velocity, filter bed dust loading on separation efficiency and filtration performance and pressure drop. Research is aimed at optimising air filters pleated filter beds in terms of improving engine performance.

Filter paper (porous material) is characterised by filtration performance  $d_z \geq 5 \mu\text{m}$ , separation efficiency at  $\varphi_w = 99.9\%$ , small thickness  $g_m = 0.4-0.8 \text{ mm}$ , and thus small  $k_m = 200-250 \text{ g/m}^2$  dust absorption limited by the permissible pressure drop  $\Delta p_{fdop}$  of the air filter [25, 26]. Filter papers stop dust grains on the fibres (which are about  $20 \mu\text{m}$  in diameter) of the porous barrier due to the various forces and filtration mechanisms. As a result, there is a continuous pressure drop across the filter (decrease in fill and engine power) until the value of  $\Delta p_{fdop}$  is reached, which is the criteria of air filter usage end and filter cartridge replacement, despite the fact that it still ensures high efficiency and filtration accuracy. It is believed that all dust grains above  $d_z \geq 1 \mu\text{m}$  cause accelerated wear of internal combustion engine components [9, 10]. The only way to protect motors against excessive wear of friction surfaces is to use materials with high efficiency and filtration accuracy. Such possibilities are created by polymer nanofibres, i.e. fibres with a diameter of less than  $1 \mu\text{m}$ . The cellulose filter material is made of fibres with relatively large diameters, usually greater than  $10 \mu\text{m}$ . A thin layer of nanofibres applied from the inlet side to a standard filter bed (e.g. cellulose) retains particles of impurities before they penetrate into the filter material. The development of fibre production technology has caused that more and more often, filter manufacturers, for example, Donaldson, Maan-Hummel, use filtration materials with an additional nano fibre layer. The dust particles retention on the surface of the layer of nanofibres allows their subsequent removal (filter cleaning) by means of reverse (in the opposite direction to the direction of airflow during operation) of a compressed air pulse under high pressure. If the dust particles are on the filter material surface, they do not damage (break) the structure of the filter cartridge when they are blown out.

In the available literature, the data characterising the properties of filtration materials with the addition of nanofibres is not very common. Hence, it is advisable to carry out experimental investigations of filtration materials with addition of nanofibres in terms of efficiency, filtration performance, and pressure drop. Such studies are expensive and labour-intensive; however, this is the most reliable research method.

## PROPERTIES OF NANO FIBRE FILTRATION MATERIALS

Nanofibres are called fibres with very small diameters, ranging from 50 to 1000 nm, depending on the production technology and material used to make them. In the textile industry, fibres with a diameter of less than 500 nm are generally considered as nanofibres. The name nanofibres is currently used for fibres produced by electrospinning [27, 28]. Nanofibres are characterised by a considerable length and a small cross-section, the diameter of which is approximately 100 times smaller than the length. Nanofibres are found in both natural materials (e.g. collagen fibres in tissues) as well as in materials produced by man. They can act as a material reinforcing the matrix in composites or can be the main component of material (fabric, non-woven).

Nanofibres have completely different properties compared to standard fibres. First of all, in relation to the mass, they have a large surface area, much higher strength, and they are also characterised by higher chemical activity and higher moisture sorption. They can be used to build filters to separate chemical or biological contaminants from the blood plasma; they can be used as gas filters—impurities with very small diameters - filters with molecular separation. Due to their structure, nanofibrous materials have unique properties and offer unexpected possibilities for their technological and commercial applications. This led to the emergence of a large number of research activities involving electrospun nanofibres for different applications such as tissue engineering and drug delivery [29, 30], enzyme immobilisation [31], acoustical damping [32], battery electrodes [33], photocatalysis [34], super-capacitors [35]. The achieved nanofibres were always accompanied by some characteristics like the very large surface area to volume ratio, flexibility in surface functionalities, superior mechanical performance, and versatility of design, which made them optimal candidates for a broad range of applications in biomedical device [36], composites [37], sensors [38], water filtration and wastewater treatment [39-41], and nano-composite membrane [42].

The development of nanofibres production technology has caused that they are more and more often used for the construction of filtration compartments of air filters in closed spaces and in the inlet air of internal combustion engines. In automotive technology, nanofibres with very small diameters of around 50-800 nm are used. For comparison [43]:

- i. human hair thickness - (20-80)  $\mu\text{m}$ ,
- ii. cellulose fibre thickness - (10-20)  $\mu\text{m}$ ,
- iii. red blood cell diameter - about 7000 nm,
- iv. width of the DNA ribbon - about 2.5 nm,
- v. diameter of silicon - about 0.23 nm.

Companies producing filter media using nanofibres have developed their own technologies for this purpose, such as Donaldson's Ultra-Web® and Fibra-Web® technology [44]. The nanofibres can be made from different polymers and thus have different physical properties. Examples of natural polymers include collagen, cellulose, silk fibroin, keratin, gelatin and polysaccharides, such as chitosan and alginate. The diameters of nanofibres depend on the type of polymer used and the production method [45, 46]. Filter media made of nanofibres are characterised by high porosity and small pore sizes. Figure 1 shows the human hair against the background of a bed of nanofibres and selected air pollutants [43].

The method of electrospinning is a widely used method of producing nanofibres [47-51]. It is a process of obtaining fibres from molten polymers or their solutions using high voltage. This modern technology, using the right polymer and dissolution system, now allows the production of fibres with diameters ranging from 3 nm to 1000 nm. Virtually any polymer can be obtained in the form of fibres by electrospinning.



**Figure 1.** Comparison of human hair on the background of nanofiber filter bed [43].

Due to the limited mechanical and strength properties of the thin layer of nanofibres (1-5  $\mu\text{m}$ ), it is applied to the substrate (as in Figure 2) from conventional filtration materials that have higher strength. The nanofibres may be laid on one or two sides of the substrate, which may be: cellulose, nylon or polyester. Usage of nanofibres, as an additional layer applied to standard filter materials for air filters used in motor vehicles, significantly increases the efficiency and accuracy of filtration.

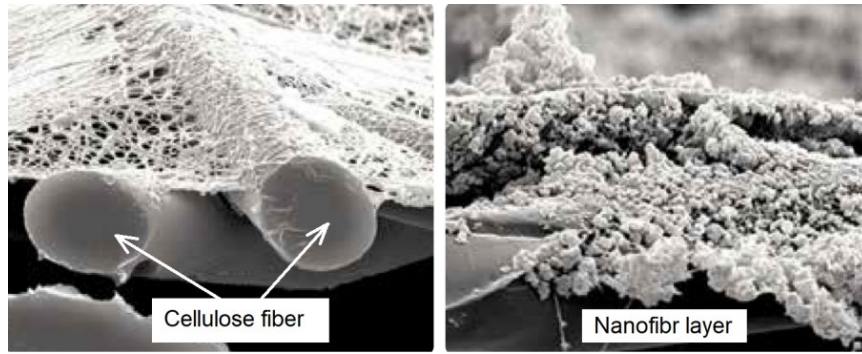


**Figure 2.** Nanofibres applied to a cellulose substrate cross-section view [44].

Figure 3 shows the fractional efficiency of a cellulose-based nanofibre filtration medium, on which a 0.3 mm nanofibre layer,  $g_m=0.1 \text{ g/m}^2$ , and fibre diameter in the range of 40-800 nm was placed [52]. The separation efficiency of the developed medium was determined using dust with a grain size of 0-10  $\mu\text{m}$ . For filtration speed,  $v_f=0.03 \text{ m/s}$ , and dust grains in the range of  $d_z=0.2\div 4.5 \mu\text{m}$ , the separation efficiency of this deposit reaches the values of  $\varphi=64\text{-}99\%$ , respectively. For a much higher filtration rate,  $v_f=0.2 \text{ m/s}$ , separation efficiency reaches a slightly lower level. These values are much higher than those based on cellulose and commercial materials with the addition of nanofibres (Figure 3). The fractional effectiveness of filters made of commercial nanofibres is practically the same as in the case of filter cartridges made of high-quality cellulose.

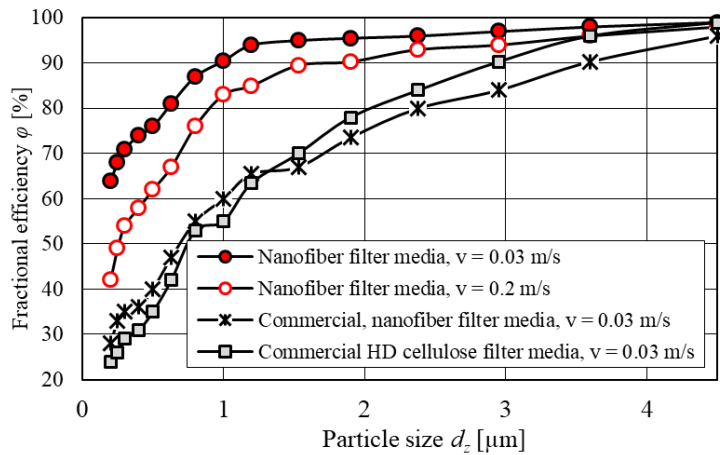


**Figure 3.** Pleated filter elements made of cellulose fibres, nanofibre layer, and cellulose fibres separation efficiency [52].

The ratio of the nanofibres to the cellulosic fibre diameter is approximately 1:130. This results in a significant increase in the filtration area for the nanofibre bed. Nanofibres area of 1 g, with a diameter of 200 nm is approximately 20  $\text{m}^2/\text{g}$ , and only 0.2  $\text{m}^2/\text{g}$  for cellulose fibres with a diameter of 20  $\mu\text{m}$ . Fibre diameter is the main variable responsible for filtration efficiency and flow resistance. The efficiency increases rapidly as the fibre diameter decreases. For example, the use of fibres with a diameter of 1  $\mu\text{m}$  instead of 50  $\mu\text{m}$  leads to an increase in filtration quality factor by 2000 [52].

Standard cellulose materials have a basis weight of approx.  $g_m=250 \text{ g/m}^2$ . The initial material effectiveness  $\varphi_0$  with nanofibres layer addition with a basis weight not exceeding  $g_m=0.1 \text{ g/m}^2$  increases by 50%, with a slight increase in pressure drop  $\Delta p$ . There is a six-time increase in the filtration quality factor  $q$  determined by the formula [53]:

$$q = \frac{-\ln \left( 1 - \frac{\varphi_0}{100} \right)}{\Delta p} \text{ (1/kPa)} \tag{1}$$

where:  $\varphi_0$  is filter bed initial efficiency (%) and  $\Delta p$  is pressure drop for the nominal airstream (kPa).

Separation efficiency, filtration performance and pressure drop of filtration materials with an additional nanofibre layer depend on the substrate structure (type of material), and the layer of nanofibres thickness. Paper [54] presents the results of filtration effectiveness tests of four samples made of different filtration materials. The novel nanofibre composites were applied on four different cloth structures, as given in Table 2. The separation efficiency of material for sample 1, 2, 3, 4 without nanofibres layer is very low, and for dust particles with dimensions below 2  $\mu\text{m}$  does not exceed 10%, as shown in Figure 4(a). Even a small layer of nanofibres ( $g_m = 0.02 \text{ g/m}^2$ ) applied to the filter bed made of these samples increases the separation efficiency of particles smaller than 2  $\mu\text{m}$  in size to over 60% as shown in Figure 4(b).

**Table 2.** Filtration materials parameters [54].

Sample	Filtration materials	Coating weight, $g_m$ ( $g/m^2$ )
1	Non-woven substrate composed of cellulose-based fibres and polymeric binders and three polyamide substrates	50
2	Knitted fabric with interlock structure	120
3	Plain weave woven fabric	140
4	Charmeuse knitted lining	50-55

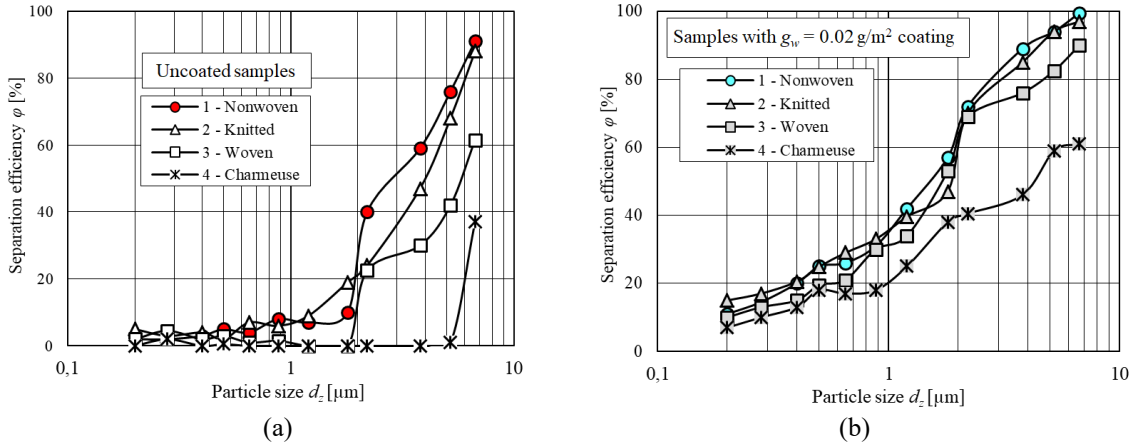


**Figure 4.** Samples 1, 2, 3, 4 filtration effectiveness of filtration material: a) without nanofibres layer, b) with nanofibres layer  $g_m = 0,02 \text{ g/m}^2$  [54].

Filtration media efficiency increases with increasing particle size (in Figure 5) regardless of the average fibre diameter. The nanofibres layer added to the original filter bed increases the filtration efficiency; the higher weight of the nanofibres layer has a higher value. The improvement is particularly important for particles smaller than  $1 \mu\text{m}$ . The addition of nanofibres layer with an average fibre diameter of  $d_{wf} = 120 \text{ nm}$  and a basis weight  $g_m = 0,03 \text{ g/m}^2$  to the bed increases the particles separation efficiency with a size of  $d_p = 0.3 \mu\text{m}$  from 12% to 42% (Figure 5a). Nanofibres layer with the basis weight  $g_m = 0.5 \text{ g/m}^2$  increased the effectiveness of these particles to 80%. Nanofibres layer of the same basis weight, but with a larger fibres diameter  $d_{wf} = 300 \text{ nm}$  improves the effectiveness of these particles only up to 50%. The largest particle  $d_p = 5 \mu\text{m}$  could be removed 100% even by the original air filter. Comparison between Figure 6(a) and 6(b) shows that an increase in the average fibre diameter from 120 to 300 nm significantly reduces the separation efficiency at all levels of mass coverage of nanofibres.

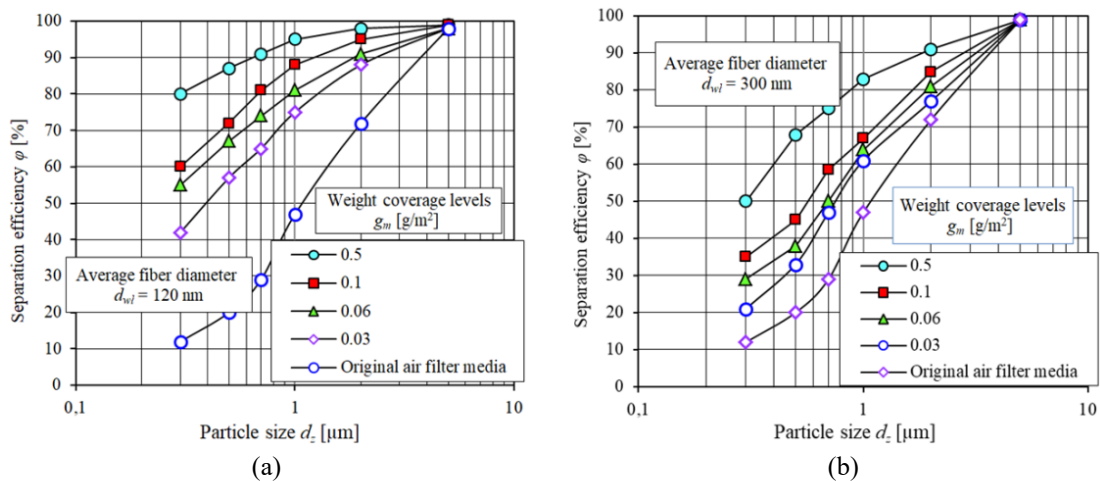


**Figure 5.** Separation efficiency of the air filter media coated with nylon-6 fibre with an average diameter of  $d_{wf}=120 \text{ nm}$  (a) and  $d_{wf}=300 \text{ nm}$  (b) at different coverage levels  $g_m$  versus the particle size [55].

In the standard filtration material, the dust grains retain deeply in the fibrous structure (depth filtration), preventing proper airflow. Nanofibres layer with a thickness of  $1.0\text{-}1.5 \mu\text{m}$  (as in Figure 6(a) and 6(b)) and PTFE membrane thickness of about  $3.8 \mu\text{m}$  (in Figure 6(c) and 6(d)) applied to the standard filtration material is aimed at stopping of particles (surface filtration) before their penetration into the cellulose standard bed. The particle distribution in two types of different filtration layers (nanofibre layer and PTFE membrane) is shown in Figure 6. Particles can get to the substrate layer with a more open structure at the deep filtration stage (marked areas in Figure 6), which results in slower clogging of the filters.

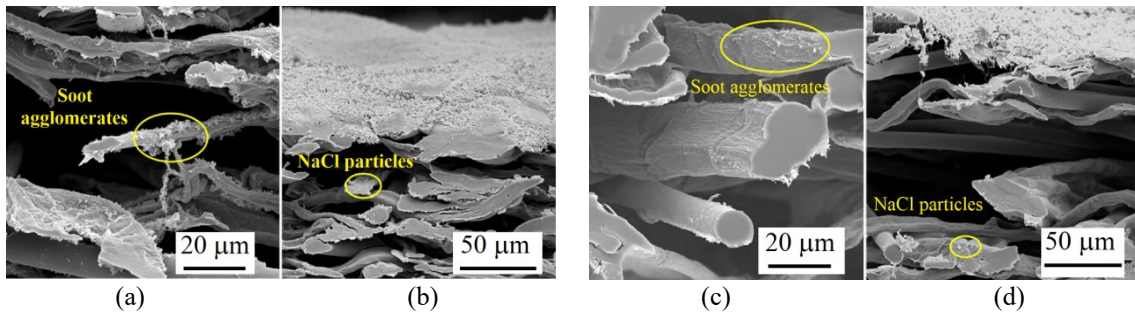


**Figure 6.** SEM image of the filter layer and particle accumulation during the filtration of various particles: (a),(c) soot agglomerates; (b),(d) NaCl particles. The loading face velocity was 0.067 m/s [56].

The dust particles stopped on the nanofibre layer surface are easily removed (filter cleaning) by a reverse stream of compressed air, in the opposite direction to the flow of the aerosol during operation as shown in Figure 7(c). If the dust particles stopped at a significant depth (Figure 7(a)) of standard filter cartridge (thickness around 0.8 mm), the return of dust particles is difficult and may damage the structure of the filter bed.

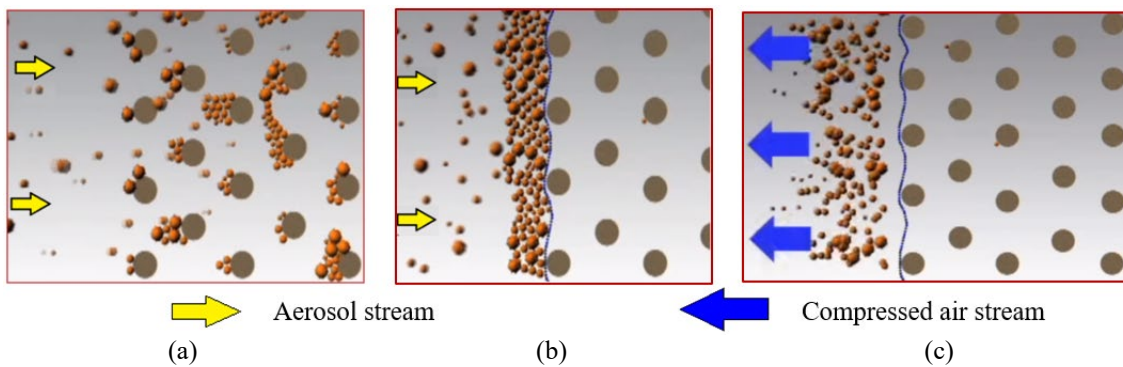


**Figure 7.** Filtration process: (a) deep filtration, (b) surface filtration with nanofibre layer, (c) during nanofibre deposit cleaning.

There are known constructional solutions for vehicle inlet air filters (Abrams M1 tank), where a filter cartridge with nanofibres and a system of automatic impulse purification of pulse jet air cleaner (PJAC) filter cartridge used. It ensures longer air filter life and thus longer vehicle life without the need to operate the filter. The principle of the PJAC operation system is that, at the time when the pressure drop of the filter inflow does not exceed the permissible value, the air filtration process takes place as in every vehicle filter. After the pressure drop reaches a certain value, a pressure modulator is activated for 0.1-0.35 s, producing a pulse in the form of compressed air with a pressure of 0.4-0.6 MPa. Compressed air flowing in the opposite direction to the airflow direction during the filtration process blows out dust particles from the surface of the filter cartridge, which then falls into the dust collector [57].

The aim of this research is to determine and compare filtration properties: efficiency and accuracy of filtration and filter cartridges flow resistance made of various filter materials (cellulose, polyester with the addition of nanofibres) by determining filtration performance  $d_{zmax}=f(k_m)$ , separation efficiency  $\varphi_w=f(k_m)$ , pressure drop  $\Delta p_w=f(k_m)$ , and flow characteristics (aerodynamic)  $\Delta p_w=f(Q_w)$  (where  $Q_w$  is the air stream flowing through the filter cartridge,  $k_m$  is the dust mass loading), dust mass  $m_w$  retained and evenly distributed over 1 m<sup>2</sup> of filter material active surface, which is expressed by the following dependence,

$$k_m = \frac{m_w}{A_w} \text{ [g/m}^2\text{]}. \tag{2}$$

The filtration speed is defined as the quotient of the air stream flowing through the filter cartridge  $Q_w$  (equal to the engine air demand) and the area of the active paper filter  $A_w$ , and is expressed by the following relationship:

$$v_{Fw} = \frac{Q_w}{A_w \times 3600} \text{ [m/s]}. \tag{3}$$

## METHODOLOGY

### Materials

The subject of the research was four filter cartridges of similar type, dimensions, filtration surface ( $A_w=0.153 \text{ m}^2$ ), but different filter material. Tested filter materials characteristic parameters are summarised in Table 3. In order to make test analysis easier, filter materials (filter cartridges) have been labelled as follows: A, B, C, D, E. Three times higher air

permeability, and double the size of the filter material A (cellulose) pores from other materials is noteworthy. On two standard filtration materials (filter cartridges D and E), there is a nanofibre layer on the inlet side. Figures 8 and 9 show SEM images from sample C and D filter material with nanofibre layer, and Figure 10 shows SEM images of filter material A (cellulose). Similar SEM images showing nanofibres layer on a standard filter bed can be found in [58, 59].

**Table 3.** Filtration materials parameters according to the manufacturer’s data.

Filter paper identification	Filtration material	Permeability, $q_p$ ( $m^3/m^2/h$ ) at 200 Pa	Permeability, $q_p$ ( $dm^3/m^2/s$ )	Grammage, $g_m$ ( $g/m^2$ )	Thickness, $g_z$ ( $\mu m$ )	Max. pore size, $d_p$ ( $\mu m$ )
A	Cellulose	-	838	121	610	79
B	Polyester	650	-	180	500	-
C	Cellulose +polyester	-	150	130	350	58
D	Cellulose +polyester + nanofibres	-	185	120	300	48
E	Polyester +nanofibres	525	-	180	500	-

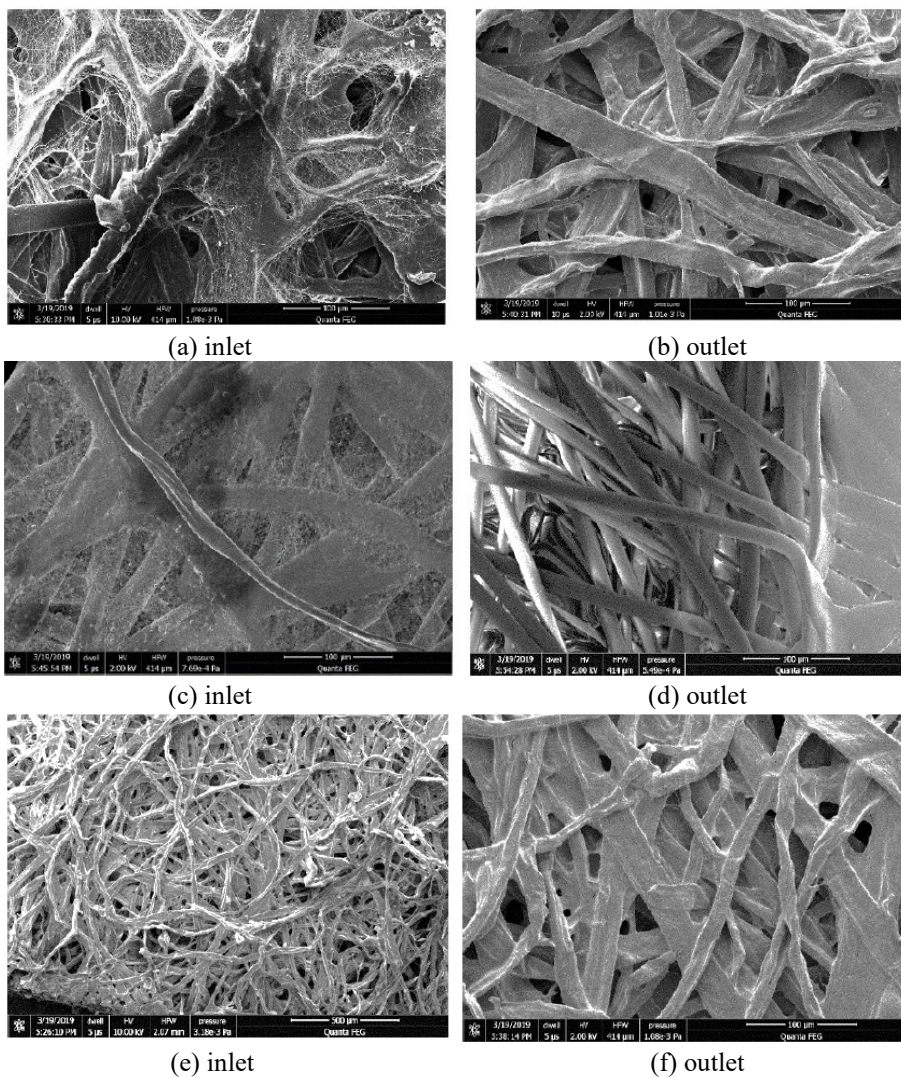


**Figure 8.** SEM images of (a),(b) cellulose + polyester + nanofibres filtration in sample C, (c),(d) polyester + nanofibres filtration in sample D and (e),(f) cellulose filtration in sample A.

**Test Condition**

Tests were carried out at the station in Figure 9, which is equipped with the Pamas-2132 particle counter and HCB-LD-2A-2000-1 sensor. The meter registers the number and size of dust grains in the air stream  $Q$ , behind the tested filter cartridge in the range of 0.7-100  $\mu m$  with  $i = 32$  measurement intervals, limited by diameters ( $d_{zimin}-d_{zimax}$ ).

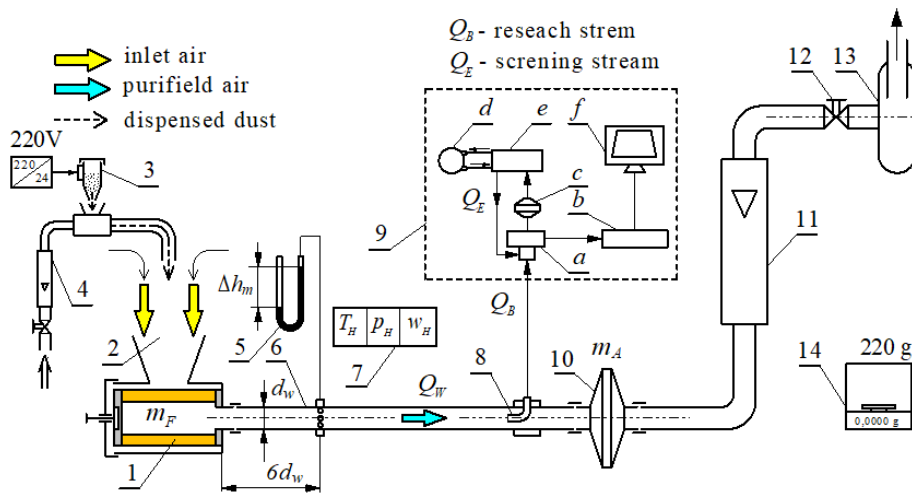


**Figure 9.** Filter cartridge test stand functional diagram.

(1 – filter cartridge, 2 – dust chamber, 3 – dust dispenser, 4 – rotameter, 5 – U-type manometer tube, 6 – measuring tube, 7 – humidity measurement set, ambient air temperature and pressure, 8 – measuring probe, 9 – particle counter (a – sensor, b – counter microprocessor, c – test stream filter, d – vacuum pump, e – flow control block, f – measuring computer), 10 – absolute filter, 11 – rotameter, 12 – airstream regulation valve, 13 – suction fan, 14 – analytical balance)

At the appropriate distance after the tested filter, the tip of the measuring probe is placed centrally in the axis of the cable, which is followed by air suction to the particle counter sensor. The measuring lead ends with a special (absolute) filter, which prevents dust from entering the rotameter, and at the same time, it is a measuring filter. The cover in which the cylindrical filter cartridge is located, PTC-D test dust is being dispensed as the national replacement for AC fine test dust, whose chemical and fractional composition is given in [60].

Cartridges filtration characteristics  $\Delta p_w = f(Q_w)$  of filter cartridges were determined in the airflow range  $Q_w = Q_{wmin} - Q_{wmax}$  or eight measuring points at equal intervals. The maximum value of the  $Q_{wmax}$  stream was determined for the assumed maximum filtration rate  $v_{Fw} = 0.1$  m/s. For passenger car filters, the maximum speed of paper filtration is in the range of 0.07-0.12 m/s [26, 61]. For the assumed filtration rate ( $v_{Fw} = 0.1$  m/s), the maximum value of the test stream calculated according to the following relationship has the value of  $Q_{wmax} = 56$  m<sup>3</sup>/h.

$$Q_{wmax} = A_w \cdot v_{Fw} \cdot 3600 \text{ [m}^3\text{/h].} \tag{5}$$

The RIN 60 rotameter with a measuring range of 3-67 m<sup>3</sup>/h and the accuracy class 2.5 was assumed for airstream measurement  $Q_w$ . Cartridges filtration characteristics; efficiency  $\varphi_w = f(k_m)$ , filtration accuracy  $d_{zmax} = f(k_m)$  and flow resistance  $\Delta p_w = f(k_m)$  were determined by the gravimetric method for a constant filtration rate  $v_{Fw} = 0.1$  m/s. Dust mass retained on the tested filter cartridge, and the absolute filter was determined in subsequent measuring cycles  $j$  with a defined duration  $\tau_p$ ; time of equal dust dosing to the filter. The concentration of dust in the inlet air to the filter cartridge  $s = 0.5$  g/m<sup>3</sup> was used. The time of equal dust dosing was set at  $\tau_p = 3$  min in the initial period (I) and  $\tau_p = 9-12$  min in the main (II) working period of filter cartridges. After each measuring cycle  $j$ , the parameters necessary to calculate: efficiency, filtration accuracy, flow resistance and filter cartridge dust absorption coefficient were determined. Dust mass retained on the tested filter cartridge, and the absolute filter was determined by an analytical balance with a measuring range of 220 g and an accuracy of 0.1 mg. During the measurement cycle (60 s before the planned end of the measurement), a procedure was started in the particle counter to measure the number and size of dust grains in the air after the filter.

After every measurement cycle  $j$  was determined:

- i. The pressure drop  $\Delta p_w$  in the cartridge was defined as the decrease of the static pressure in the outlet pipe at a distance of  $6d_w$  from the edge of the cartridge outlet on the basis of the  $\Delta h_{mj}$  (mm H<sub>2</sub>O) indicator on the U-tube liquid manometer, according to the relationship:

$$\Delta p_{wj} = \frac{\Delta h_{mj}}{1000} \cdot (\rho_m - \rho_H) \cdot g \text{ (Pa)} \tag{6}$$

where  $\rho_m$  is manometric liquid density (kg/m<sup>3</sup>),  $\rho_H$  is air density (kg/m<sup>3</sup>) and  $g$  is gravity acceleration (m/s<sup>2</sup>).

- ii. The filter filtration efficiency, as the quotient of the dust mass  $m_{ZFj}$  stopped by the filter and the dust mass  $m_{Dj}$  introduced into the filter during the subsequent measurement cycle  $j$  based on the dependence:

$$\varphi_j = \frac{m_{Fj}}{m_{Dj}} = \frac{m_{Fj}}{m_{Fj} + m_{Aj}} 100\% \tag{7}$$

iii. Dust mass loading  $k_{mj}$  of examined filtration material

$$k_{mj} = \frac{\sum_{j=1}^n m_{Fj}}{A_w} (g/m^2) \tag{8}$$

- iv. Number of dust grains  $N_{zi}$  in the air stream after the filter (passed through the filter material) in the measurement intervals limited by diameters ( $d_{zimin}-d_{zimax}$ ).
- v. Filtration accuracy, as the largest size of dust grain  $d_{zj} = d_{zimax}$  in the air stream after the filter.
- vi. Percentage of individual fractions of dust grains in the air after the filter for a given test cycle:

$$U_{zi} = \frac{N_{zi}}{N_z} = \frac{N_{zi}}{\sum_{i=1}^{32} N_{zi}} 100\% \tag{9}$$

where:  $N_z = \sum_{i=1}^{32} N_{zi}$  – total number of dust grains passed through the filter (from all measuring compartments) in the test cycle.

During the tests, a research cycle was used in which five counts of dust grains in the range of 0.7-20  $\mu\text{m}$  were programmed, which were divided into 20 identical measurement intervals limited by diameters ( $d_{zimin}-d_{zimax}$ ) with pitch;  $\Delta d_{zi} = 0.4 \mu\text{m}$  (0.7-1.1  $\mu\text{m}$ ; 1.1-1.5  $\mu\text{m}$ ; 1.5-1.9  $\mu\text{m}$ ; ...; 8.3-8.7  $\mu\text{m}$ ) and 11 measuring compartments limited by diameters ( $d_{zimin}-d_{zimax}$ ) with a pitch;  $\Delta d_{zi} = 0.8 \mu\text{m}$  (8.7-9.5  $\mu\text{m}$ ; 9.5-10.3  $\mu\text{m}$ ; 10.3-11.1  $\mu\text{m}$ ; ...; 15.9-16.7  $\mu\text{m}$ ). The last measuring range had a range of  $\Delta d_{zi} = 6.7-20.0 \mu\text{m}$ .

## RESULTS AND DISCUSSION

The tested filter cartridges flow characteristics  $\Delta p_w = f(Q_w)$  are shown in Figure 10. In line with the airflow increase, there is a parabolic increase in the flow resistance  $\Delta p_w = f(Q_w)$ , consistent with the literature information. The highest flow resistance values in the entire  $Q_w$  airflow range were recorded for filter cartridge D made of a material that is a composite layer of cellulose, polyester and nanofibres. For  $Q_{wmax} = 56 \text{ m}^3/\text{h}$ , the flow resistance of cartridge D is  $\Delta p_w = 498.5 \text{ Pa}$  (as in Figure 10). The lower value of the flow resistance  $\Delta p_w$  (by 6%) is characterised by filtration cartridge C, which filtration material is a composite of cellulose and polyester layers (without nanofibres). Cartridge A, which filtering material is exclusively cellulose paper, achieves the lowest flow resistance value  $\Delta p_w = 344.1 \text{ Pa}$ . This value is 30% lower than the flow resistance of cartridge C, where a layer of nanofibres is applied to the standard filter bed (cellulose and polyester). This is due to the much larger (three times) permeability of the cellulose bed  $q_p = 838 \text{ dm}^3/\text{m}^2/\text{s}$  than the deposit D being a composite of cellulose + polyester + nanofibres layers.

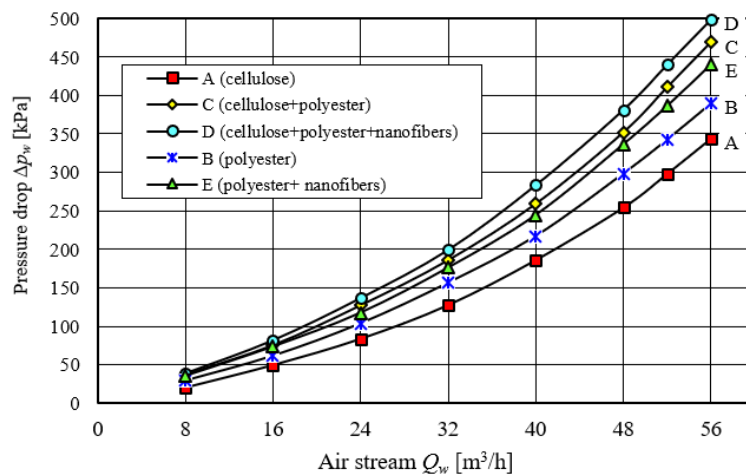


Figure 10. Flow characteristics  $\Delta p_w = f(Q_w)$  of tested filter cartridges.

Cartridge E with polyester + nanofibres filter material achieves a flow resistance  $\Delta p_w = 439.9 \text{ Pa}$  at  $Q_{wmax} = 56 \text{ m}^3/\text{h}$ , while B cartridge, made only from polyester, obtains a resistance  $\Delta p_w = 389.1 \text{ Pa}$ , which is 11.5% lower. The above results indicate that the filter bed being a composite of several layers of different materials, including nanofibres, achieves higher flow resistance values than cellulose material which is two times thicker. Test results separation efficiency  $\varphi_f$ , filtration

performance  $d_{zmax}$ , and pressure drop  $\Delta p_f$  calculations of tested filtration materials are shown in Figure 11 and 12. As the dust mass retained in the filtration layer increases ( $k_m$  – dust mass loading), the filtration efficiency, filtration performance and pressure drop of filter cartridges assume increasing values. This results from the space-filling between the fibres (pores), which is consistent with the literature [26, 52, 61].

The work of tested filter cartridges can be divided into two stages. It was assumed that the initial stage (I) of filter cartridges operation lasts until the separation efficiency stabilises at the level of  $\varphi_w = 99.9\%$ . This stage is characterised by low initial efficiency, filtration performance, and low-pressure drop. The duration has a different value for each step.

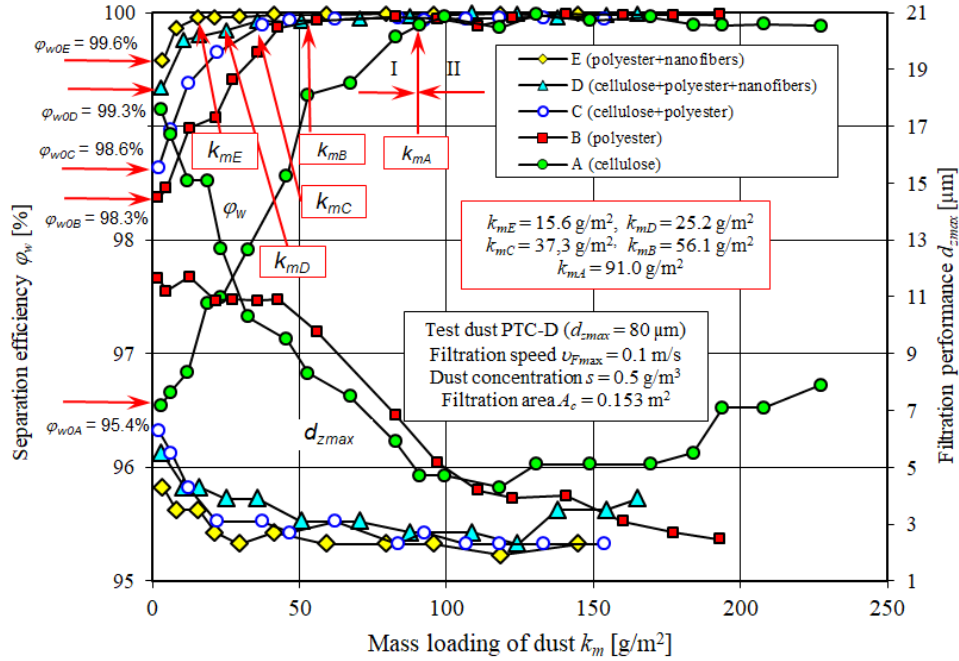


Figure 11. Separation efficiency  $\varphi_w$  and filtration performance  $d_{zmax}$  depending on the tested filter cartridges dust mass loading  $k_m$ .

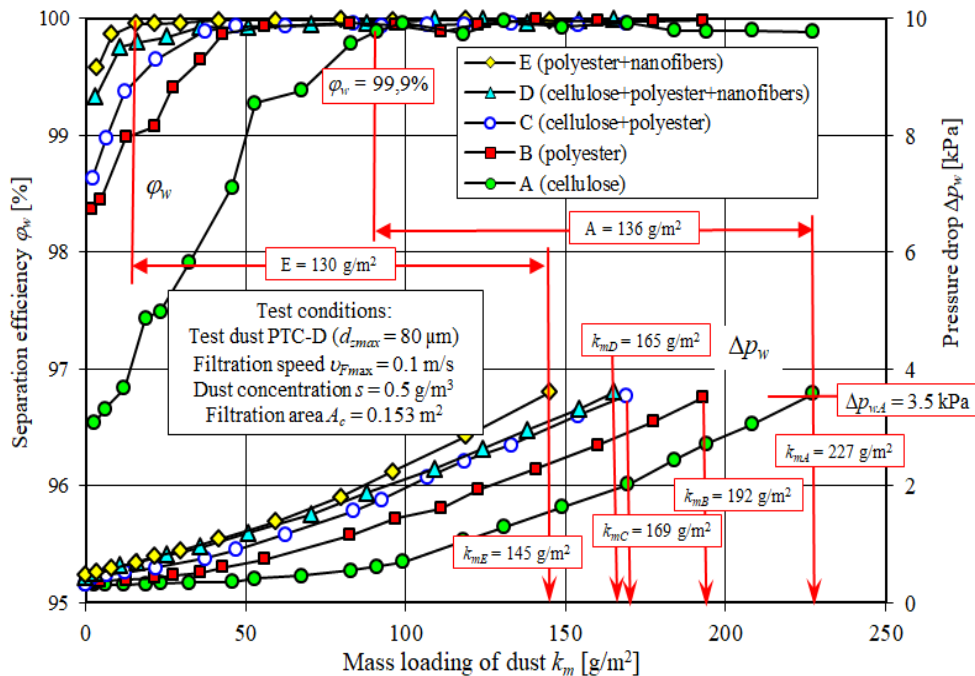


Figure 12. Separation efficiency  $\varphi_w$  and pressure drop  $\Delta p_w$  depending on the tested filter cartridges dust mass loading  $k_m$ .

For cellulose filter cartridge A, the initial separation efficiency is  $\varphi_{wA}=96.5\%$ , and the maximum grain size does not exceed the value of  $d_{zmaxA}=17.6 \mu\text{m}$ . The determined value of separation efficiency ( $\varphi_w=99.9\%$ ) is achieved at the dust mass loading  $k_{mA}=91 \text{ g/m}^2$ , while the pressure drop increase is insignificant. For cartridges made of other filtration materials, the first stage is much shorter. For polyester insert B, stage (I) ends with a dust mass loading  $k_{mB}=56.1 \text{ g/m}^2$ ,

while for cartridge C (cellulose + polyester)  $k_{mC}=37.3 \text{ g/m}^2$ , and for D (cellulose + polyester + nanofibres) coefficient  $k_{mD}=25.2 \text{ g/m}^2$ . In cartridge E (polyester + nanofibres), stage I last the shortest. Cartridge achieves efficiency  $\varphi_{wE}=99.9\%$  for coefficient  $k_{mD}=15.6 \text{ g/m}^2$ .

The initial separation efficiency for the mentioned cartridges is assumed to be higher respectively;  $\varphi_{w0B}=98.3\%$ ,  $\varphi_{w0C}=98.6\%$ ,  $\varphi_{w0D}=99.3\%$ ,  $\varphi_{w0E}=99.6\%$ . At the end of the first stage filtration, the sizes of the maximum grains for A, B, C, D, E contributions are stabilised at the following level:  $d_{zmaxA}=4.7 \text{ }\mu\text{m}$ ,  $d_{zmaxB}=3.9 \text{ }\mu\text{m}$ ,  $d_{zmaxC}=3.1 \text{ }\mu\text{m}$ ,  $d_{zmaxD}=3.9 \text{ }\mu\text{m}$ ,  $d_{zmaxE}=3.5 \text{ }\mu\text{m}$ . The initial work stage of the A cartridge made of cellulose is several times longer than insert D (polyester with a layer of nanofibres) and C (cellulose + polyester + nanofibres). At the same time, the required high separation efficiency of the inserts with nanofibre layer reach much earlier than cartridges made of standard filter material. This confirms the literature about the positive nanofibres influence on the filtration efficiency and filtration performance materials used in the automotive industry.

In stage (I) of filtration, the dirt particles were deposited on the surface of the fibres of the porous structure and on previously deposited particles. In this way, they form slowly growing complicated dendritic structures (agglomerates), which fill free spaces between fibres. They reduce the flow area around the fibres. In response to changes in the filter structure, there are changes in the airflow. The flow velocity of the aerosol increases, which increases the flow resistance through the filter bed. In the second (II) stage of the filtration cartridges, the separation efficiency remains unchanged, stabilised  $\varphi_w=99.9\%$ . In contrast, the pressure drop reaches higher values, but the intensity of growth is greater for inserts made of materials with nanofibres addition.

Cartridges with a nanofibre layer have lower dust absorption. It is determined by surface filtration, as a result of which dust grains did not penetrate deep into the deposit but stopped mostly on the nanofibre layer. When the flow resistance  $\Delta p_{maxE}=3.5 \text{ kPa}$  is achieved, the tested filter cartridges retain and accumulate different dust masses. Filter insert A achieves absorption coefficient  $k_{mA}=227 \text{ g/m}^2$ , while for insert E,  $k_{mE}=145 \text{ g/m}^2$  (as in Figure 12). However, the unit dust mass  $k_m$  accumulated on the filter cartridges, from the moment the cartridge achieves efficiency  $\varphi_w=99.9\%$  until the flow resistance  $\Delta p_{maxE}=3.5 \text{ kPa}$  is similar and assumes a value of about  $135 \text{ g/m}^2$  (shown in Figure 12). It depends on the length of the initial period (I), which lasts until the insert efficiency of  $\varphi_w=99.9\%$  reached. During this period, dust particles of considerable size are in the air behind the filter ( $d_{zmaxA} = 7\text{-}18 \text{ }\mu\text{m}$ ), which adversely affects the durability of the engine. For cartridges (E and D) with nanofibre layer, this period lasts shorter and represents 10% and 15% of the total insert working time, respectively. For standard insert A, the initial period (I) represents over 40% of the total insert working time and, therefore, has a significant impact on the abrasive wear of engine components.

Filter elements made of cellulose composite and polyester, together with the applied layer of nanofibres, are characterised by higher efficiency and filtration performance in the whole range of work (smaller dust grain sizes  $d_{zmax}$  in the air behind the filter cartridge) than inserts made of filter material without a layer of nanofibres. Filter inserts with a nanofibre layer obtain a maximum mass loading of dust of  $k_m=145\text{-}175 \text{ g/m}^2$ . For a similar pressure drop value  $\Delta p_{wdop}$  (of about 4 kPa), filter cartridges without nanofibres layer obtain dust mass loading in the range of  $k_m=153\text{-}243 \text{ g/m}^2$ , which is 50% more value. This is due to the lower pressure drop intensity of the filter cartridges without the nanofibres layer. After the filtration inserts with nanofibre layer have a pressure drop of 4 kPa, the phenomenon of dust agglomeration from the filter bed is observed. This proves that in filter beds with nanofibre layer, mainly surface filtration occurs, not deep.

Low efficiency and filtration performance in the initial period of filter cartridges work without nanofibres layer (this is the case after replacing a contaminated filter cartridge with a new one) causes that dust particles larger than  $5 \text{ }\mu\text{m}$  in the air entering the engine can have a significant impact on accelerated wear of engine components, mainly cylinder funnel-piston ring-cylinder. Such a phenomenon is not observed when using filter cartridges with a layer of nanofibres.

In the final stage of filtration, large dust grains (of  $d_{zmaxA}=7.9 \text{ }\mu\text{m}$ ) are found in the air behind the filter cartridge A. There is also a noticeable decrease in cartridge filtration (Figure 11). This indicates that the grains have passed to the outlet side of the filter material. In the final stage, a significant dust mass is accumulated in the form of expanded tree-like dendrites. The dust grains located at the top of the dendrites are entrained and transferred to the outlet side of the filter material. As a result of this phenomenon, along with the inlet air, dust flows into the engine cylinders. Measurement results of dust grains numbers in the air after the tested filter cartridge (passed through the filter material) are shown in Figure 13 and 14.

The largest part in the air  $U_p$  is made of dust grains with dimensions of  $d_z=0.7\text{-}1.1 \text{ }\mu\text{m}$ . Their participation in the air behind the tested filter cartridge A (cellulose) is much smaller than for cartridge D (cellulose+polyester+nanofibres). After the first measurement for filter cartridge D, its value is  $U_p=71.4\%$ , and for cartridge A,  $U_p=27.3\%$  (Figure 13). For other measuring intervals, as the size of the grain increases, the number of dust grains decreases, which indicates the increasing separation efficiency of the tested material. In the last measurement interval, there is usually one dust grain with the largest size  $d_z=d_{zmax}$  being the criterion of separation efficiency (Figure 14).

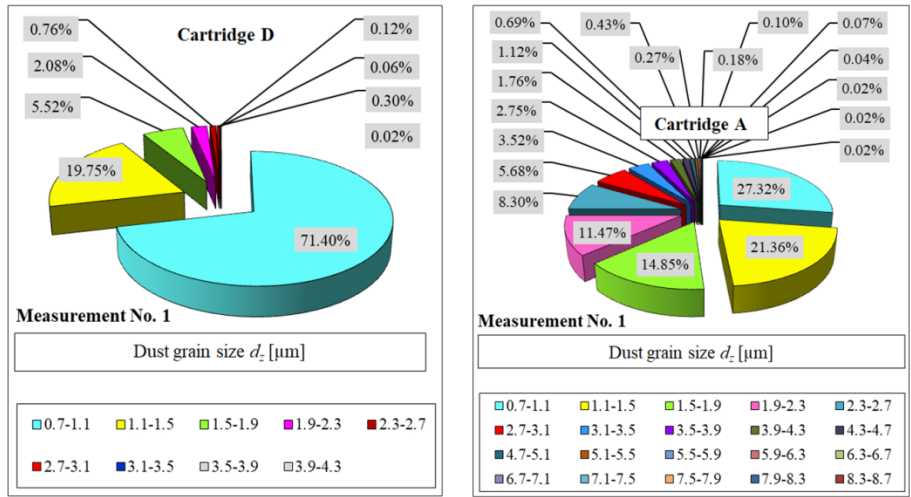


**Figure 13.** Granular composition of dust grains assumed by the filter cartridge (a) D (cellulose+polyester+nanofibres) after reaching dust mass loading  $k_{mD} = 3 \text{ g/m}^2$ , (b) A (cellulose) after reaching the dust mass loading  $k_{mA} = 2.8 \text{ g/m}^2$ .

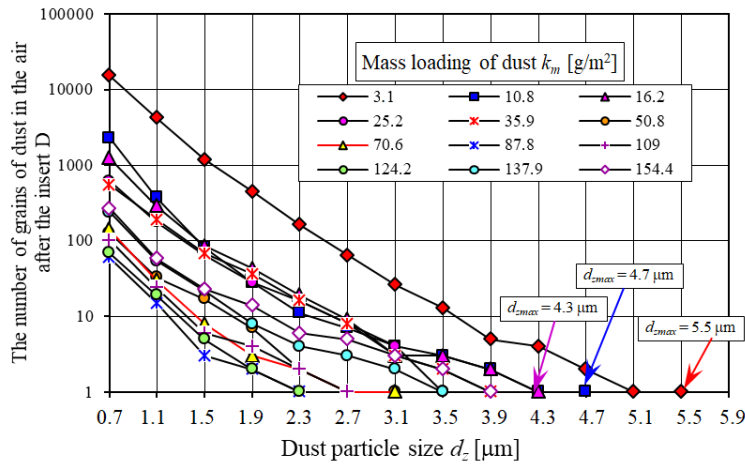


**Figure 14.** The number of dust grains in subsequent measurement intervals registered in the air after the filter cartridge D (cellulose + polyester + nanofibres).

The results of the calculations presented in Figure 15 show that the highest value of the quality coefficient  $q=12.6 \text{ kPa}^{-1}$  obtained by sample E (polyester + nanofibre), which also achieves the highest initial efficiency  $\phi_{0wE}=99.6\%$  and the accuracy of filtration  $d_{maxE}$  below  $4.3 \mu\text{m}$ . A definite lower value of the quality coefficient  $q=9.7 \text{ kPa}^{-1}$  obtained by sample A (cellulose), which results mainly from lower initial separation efficiency  $\phi_{0wA}=99.6\%$ .

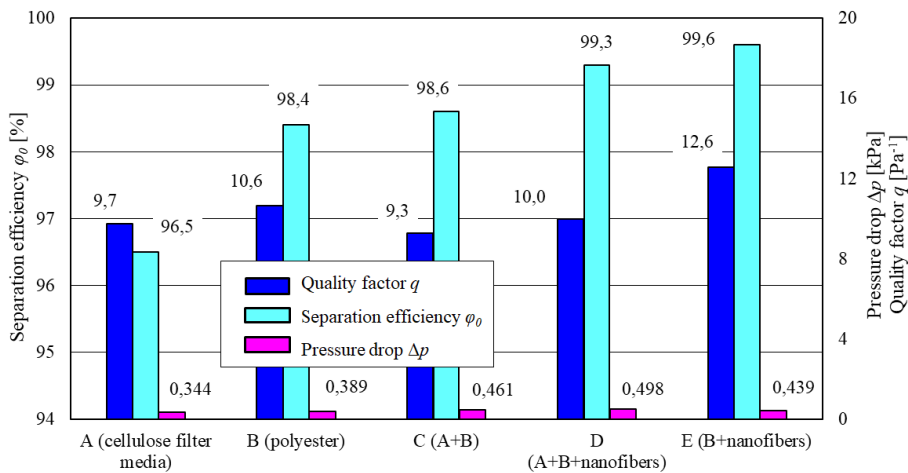


**Figure 15.** Filtration effectiveness of tested materials A, B, C, D, E used in internal combustion engines air filters.

## CONCLUSION

- i. Nanofibres layer with a thickness of about few micrometres applied to the substrate from conventional filter materials of motor vehicles air filters, increases the effectiveness of  $\varphi_w$  and filtration accuracy  $d_{zmax}$ , especially in the initial filtration period and a slight pressure drop  $\Delta p_w$  in cartridges, which confirms with the literature. The filtration inserts with a nanofibre layer reached the initial separation efficiency of  $\varphi_{w0E}=99.6\%$  and  $\varphi_{w0D}=99.3\%$  and the accuracy of  $d_{zmaxE}=4.3 \mu\text{m}$ ,  $d_{zmaxD}=5.5 \mu\text{m}$  respectively. Cartridges from standard filtration material (cellulose, polyester) obtain much lower values of filtration effectiveness ( $\varphi_{w0A}=95.4\%$ ,  $\varphi_{w0B}=98.3\%$ ) and accuracy ( $d_{zmaxA}=17.6 \mu\text{m}$ ,  $d_{zmaxB}=12.7 \mu\text{m}$ ).
- ii. With the increase of dust mass retained on the filter cartridge (increase of absorption coefficient  $k_m$ ), a rapid increase in the separation efficiency of the tested cartridges takes place in the initial period. Due to the higher value of the initial separation efficiency of cartridges with the addition of nanofibres, the working time of these cartridges until the contractual value of separation efficiency reached at  $\varphi_w=99.9\%$  (initial filtration period) is several times shorter than cartridges from standard filtration materials. The longer initial filtration period means that a larger mass of high-volume mineral dust is sucked into the engine cylinders together with the air. This phenomenon is influenced by accelerated wear of engine components and durability.
- iii. Filter cartridges with nanofibres layer have a higher intensity of flow resistance  $\Delta p_w$  than filter cartridges without this layer, and after reaching the value of  $\Delta p_{wdop}$  about 3.5 kPa they obtain a dust absorption coefficient of  $k_m=145-165 \text{ g/m}^2$ . For a similar resistance value  $\Delta p_{wdop}$ , filter cartridges without a layer of nanofibres obtain a dust absorption coefficient within the limits of  $k_m=169-227 \text{ g/m}^2$ , so 50% higher value. This is due to the fact that filter cartridges with a layer of nanofibres accumulate dust on the surface, thereby blocking the airflow through the layer, which reflected in the higher intensity of the flow resistance increase. It proves that in filter beds with a layer of nanofibres, mainly surface filtration occurs, not a deep one.
- iv. At the value of flow resistance of 3.5 kPa, the phenomenon of falling off the dust agglomerates from the filtration bed surface is observed in the tested inserts with the addition of nanofibres. This confirms the possibility of removing the dust accumulated on the surface of the cartridge through the impulse of the compressed air stream, and thus prolong several times life of the air filter.

## REFERENCES

- [1] Barris MA. Total Filtration™: The influence of filter selection on engine wear, emissions, and performance. SAE Technical Paper: 952557; 1995.
- [2] Barbolini M, Di Pauli F, Traina M. Simulation of Air Filtration for Determination of Filter Elements. MTZ - Motor Technology Magazine 2014; 75(11): 52-57.
- [3] Bojdo N. Rotorcraft engine air particle separation. PhD Thesis, University of Manchester, UK, 2012.
- [4] Szczepankowski A, Szymczak J, Przysowa R. The effect of a dusty environment upon performance and operating parameters of aircraft gas turbine engines. In: Specialists' Meeting - Impact of Volcanic Ash Clouds on Military Operations NATO AVT-272-RSM-047, Vilnius, Lithuania; May, 2017.
- [5] Abd Halim MA, Nik Mohd NAR, Mohd Nasir MN, Dahalan MN. Experimental and numerical analysis of a motorcycle air intake system aerodynamics and performance. International Journal of Automotive and Mechanical Engineering 2020; 17(1): 7607-7617.
- [6] Mustafa NS, Ngadiman NHA, Abas MA, Noordin MY. Application of Box-Behnken analysis on the optimisation of air intake system for a naturally aspirated engine. International Journal of Automotive and Mechanical Engineering 2020; 17(2): 8029-8042.
- [7] Tang R-J, Hu B-F, Zhang M, Lu Z-J. Study on separation characteristics of dust and droplet on air intake pre-filtration systems of CV based on CFD simulation and test. In: International Conference on Artificial Intelligence and Computing Science (ICAICS 2019), Hang Zhou, China; 24-25 March, 2019.
- [8] Long J, Tang M, Sun Z, et al. Dust loading performance of a novel submicro- fibre composite filter medium for engine. Materials 2018; 11: 2038.
- [9] Lakshminarayanan PA, Nayak NS. Critical component wear in heavy duty engines. 1st ed., Singapore: John Wiley & Sons (Asia) Pte Ltd., 2011.
- [10] Wróblewski P, Iskra A. Geometry of shape of profiles of the sliding surface of ring seals in the aspect of friction losses and oil film parameters. Combustion Engines 2016; 167(4): 24-38.
- [11] Dahlan AA, Muhammad Said MF, Abdul Latiff Z, et al. Acoustic study of an air intake system of si engine using 1-dimensional approach. International Journal of Automotive and Mechanical Engineering 2019; 16(1): 6281-6300.
- [12] Sawant P, Bari S. Effects of variable intake valve timings and valve lift on the performance and fuel efficiency of an internal combustion engine. SAE Technical Paper: 2018-01-0376; 2018.
- [13] Chhalotre S, Baredar P, Soni S. Experimental investigation to analyse the effect of variation in intake air temperature on the throttle response of the SI engine. International Journal of Mechanical Engineering and Technology 2018; 9(7): 972-981.

- [14] Sawant P, Bari S. Combined effects of variable intake manifold length, variable valve timing and duration on the performance of an internal combustion engine. In: ASME 2017 International Mechanical Engineering Congress and Exposition, Tampa, Florida, USA; 3-9 November, 2017.
- [15] Hanriot S de M, Queiroz JM, Maia CB. Effects of variable-volume Helmholtz resonator on air mass flow rate of intake manifold. *Journal of the Brazilian Society of Mechanical Sciences and Engineering* 2019; 41: 78.
- [16] Aradhye O, Bari S. Continuously varying exhaust pipe length and diameter to improve the performance of a naturally aspirated SI engine. In: International Mechanical Engineering Congress and Exposition IMECE2017, Tampa, Florida, USA; 3-9 November, 2017.
- [17] Kang JH, Ih JG. Acoustical characteristics of the air filter in the engine intake air cleaner. *International Journal of Automotive Technology* 2018; 19(6): 981-991.
- [18] Allama S, Elsaid AM. Parametric study on vehicle fuel economy and optimisation criteria of the pleated air filter designs to improve the performance of an IC diesel engine: Experimental and CFD approaches. *Separation and Purification Technology* 2020; 241: 116680.
- [19] Barbolini M, Pauli FD, Traina M. Simulation of air filtration for the determination of filter elements. *Auto Tech Review* 2016; 12: 25-28.
- [20] Feng Z, Pan W, Wang Y, Long Z. Modeling filtration performance of pleated fibrous filters by Eulerian-Markov method. *Powder Technology* 2018; 340: 502-510.
- [21] Théron F, Joubert A, Coq LL. Numerical and experimental investigations of the influence of the pleat geometry on the pressure drop and velocity field of a pleated fibrous filter. *Separation and Purification Technology* 2017; 182: 69-77.
- [22] Li S, Hu S, Xie B, et al. Influence of pleat geometry on the filtration and cleaning characteristics of filter media. *Separation and Purification Technology* 2019; 210: 38-47.
- [23] Maddineni AK, Das D, Damodaran RM. Numerical investigation of pressure and flow characteristics of pleated air filter system for automotive engine intake application. *Separation and Purification Technology* 2019; 212: 126-134.
- [24] Saleh AM, Tafreshi HV, Pourdeyhimi B. An analytical approach to predict pressure drop and collection efficiency of dust-load pleated filters. *Separation and Purification Technology* 2016; 161: 80-87.
- [25] Dziubak T. Problems of dust removal from multi-cyclones of engine air cleaners in cross-country motor vehicles. *The Archives of Automotive Engineering* 2017; 76(2): 37-62.
- [26] Dziubak T, Szwedkiewicz S. Operating properties of non-woven fabric panel filters for internal combustion engine inlet air in single and two-stage filtration systems. *Eksplotacja i Niezawodność – Maintenance and Reliability* 2015; 17(4): 519-527.
- [27] Kenry, Lim CT. Nano fibre technology: current status and emerging developments. *Progress in Polymer Science* 2017; 70: 1-17.
- [28] Yalcinkaya F. Preparation of various nano fibre layers using wire electrospinning system. *Arabian Journal of Chemistry*. 2017; 12: 5162-5172.
- [29] Daristotle JL, Behrens AM, Anthony D. et al. A review of the fundamental principles and applications of solution blow spinning. *ACS Applied Materials Interfaces* 2016; 8: 34951-34963.
- [30] Xue J, Wu T, Dai Y, Xia Y. Electrospinning and electrospun nanofibres: Methods, materials, and applications. *Chemical Reviews* 2019; 119: 5298-5415.
- [31] Li W, Shi J, Zhao Y, et al. Bioinspired synthesis of nanofibres on monolithic scaffolds for enzyme immobilisation with enhanced loading capacity and activity recovery. *Journal Chemical Technology and Biotechnology* 2019; 94: 3763-3771.
- [32] Yu PP, Wang Z, Lu S, Lai P. Effects of carbon nanofibres and carboxyl functionalized multi-walled carbon nanotubes on mechanical damping behavior of cement. *Journal of Nanoscience and Nanotechnology* 2019; 19: 163-169.
- [33] Zhang L, Huang Y, Miao YE, et al. Hierarchical composites of NiCo<sub>2</sub>S<sub>4</sub> nanorods grown on carbon nanofibres as anodes for high-performance lithium ion batteries. *Composites Communications* 2020; 21:100395.
- [34] Al-Enizi AM, El-Halwany MM, Al-Abdrabnabi MA, et al. A novel low temperature route to produce CdS/ZnO composite nanofibres as effective photocatalysts. *Catalysts* 2020; 10(4): 417.
- [35] Uppugalla S, Srinivasan P. Polyaniline nanofibres and porous Ni(OH)<sub>2</sub> sheets coated carbon fabric for high performance super capacitor. *Journal of Applied Polymer Science* 2019; 136(41): 48042-48052.
- [36] Villarreal-Gómez LJ, Cornejo-Bravo JM, Graziano RV, Grande D. Electrospinning as a powerful technique for biomedical applications: a critically selected survey. *Journal of Biomaterials Science, Polymer Edition* 2016; 27(2): 157-176.
- [37] Anjabin R, Khosravi H. Property improvement of a fibrous composite using functionalised carbon nanofibres. *Polymer Composites* 2019; 40(11): 4281-4288.
- [38] Terra IAA, Sanfelice RC, Scagion VS, et al. Polyvinylpyrrolidone electrospun nanofibres doped with Eu<sup>3+</sup>: Fabrication, characterisation, and application in gas sensors. *Journal of Applied Polymer Science* 2019 136(29); 47775-47782.
- [39] Liao Y, Loh CH, Tian M, et al. Progress in electrospun polymeric nanofibrous membranes for water treatment: Fabrication, modification and applications. *Progress in Polymer Science* 2018; 77: 69-94.
- [40] Said KAM, Jamain RL, Sutan NSM, Alipah NAM. Enhanced permeation performance with incorporation of silver nitrate onto polymeric membrane. *Journal of Mechanical Engineering and Sciences* 2018; 12(3): 3811-3824.
- [41] Roslan NSA, Abdul Hamid N, Md Isa MH, et al. Nylon electrospun nanofibre water filtration media for wastewater treatment. *Materials Research Express* 2018; 5(10): 105010.

- [42] Nemavhola F, Sigwadi R. Prediction of hyperelastic material properties of Nafion117 and Nafion/ZrO<sub>2</sub> nano-composite membrane. *International Journal of Automotive and Mechanical Engineering* 2019; 16(2): 6524-6540.
- [43] Kattamuri SBK, Potti L, Vinukonda A, et al. Nanofibres in pharmaceuticals - A review. *American Journal of PharmTech Research* 2012; 2(6): 187-212.
- [44] Donaldson Company, Inc. Ultra-Web-Media. Retrieved from <https://www.donaldson.com/pl-pl/industrial-dust-fume-mist/technical-articles/ultra-web-media-technology/>; 8 October, 2020.
- [45] Haider A, Haider S, Kang I-K. A comprehensive review summarising the effect of electrospinning parameters and potential applications of nanofibres in biomedical and biotechnology. *Arabian Journal of Chemistry* 2018; 11(8): 1165-1188.
- [46] Ismail N, Maksoud FJ, Ghaddara N, et al. A mathematical model to predict the effect of electrospinning processing parameters on the morphological characteristic of nanofibrous web and associated filtration efficiency. *Journal of Aerosol Science* 2017; 113: 227-241.
- [47] Ahne J, Li Q, Croiset E, Tan Z. Electrospun cellulose acetate nanofibres for airborne nanoparticle filtration. *Textile Research Journal* 2019; 89(15): 3137-3149.
- [48] Buivydiene D, Krugly E, Ciuzas D, et al. Formation and characterisation of air filter material printed by melt electrospinning. *Journal of Aerosol Science* 2019; 131: 48-63.
- [49] Givehchi R, Li Q, Tan Z. Filtration of sub-3.3 nm tungsten oxide particles using nanofibrous filters. *Materials* 2018; 11: 1277.
- [50] Nie J, Wang ZL, Li JF, et al. Interface hydrogen-bonded core-shell nanofibres by coaxial electrospinning. *Chinese Journal of Polymer Science* 2017; 35(8) 1001-1008.
- [51] Nie HR, Wang C, He AH. Fabrication and chemical crosslinking of electrospun trans-polyisoprene nano fibre nonwoven. *Chinese Journal of Polymer Science* 2016; 34(6): 697-708.
- [52] Jaroszczyk T, Petrik S, Donahue K. Recent development in heavy duty engine air filtration and the role of nano fibre filter media. *Journal of KONES - Powertrain and Transport* 2009; 16(4): 207-216.
- [53] Kim HB, Lee WJ, Choi SC, et al. Dependence of the fibre diameter on quality factor of filters fabricated with meta-aramid nanofibres. *Separation and Purification Technology* 2019; 222: 332-341.
- [54] Heikkilä P, Sipilä A, Peltola M, Harlin A. Electrospun PA-66 coating on textile surfaces. *Textile Research Journal* 2007; 77(11): 864-870.
- [55] Li L, Frey MW, Green TB. Modification of air filter media with nylon-6 nanofibres. *Journal of Engineered Fibres and Fabrics* 2006; 1(1): 1-2.
- [56] Sun Z, Liang Y, He W, et al. Filtration performance and loading capacity of nano-structured composite filter media for applications with high soot concentrations. *Separation and Purification Technology* 2019; 221: 175-182.
- [57] Li S, Wang F, Xin J, et al. Study on effects of particle size and maximum pressure drop on the filtration and pulse-jet cleaning performance of pleated cartridge filter. *Process Safety and Environmental Protection* 2019; 123: 99-104.
- [58] Givehchi R, Li Q, Tan Z. Filtration of sub-3.3 nm tungsten oxide particles using nanofibrous filters. *Materials* 2018; 11(8) 1277.
- [59] Yu J, Liang Y, Tang M. A novel energy-efficient kapok filter paper with high DHC for solid-oil mixed aerosol: Performance and loading behavior evolution mechanism. *Separation and Purification Technology* 2020; 235: 116180.
- [60] PN-ISO 5011:1994. Air filters for internal combustion engines and compressors, Research and activities, PKN, Warsaw 1994 (in Polish).
- [61] Dziubak T, Bąkała L. Experimental research of the material filtration characteristics with nanofibres addition. *Journal of KONES - Powertrain and Transport* 2018; 25(4): 83-94.